THE JOURNAL OF PHYSICAL CHEMISTRY B

Article

pubs.acs.org/JPCB

High-Precision Temperature Determination of Evaporating Light-Absorbing and Non-Light-Absorbing Droplets

G. Derkachov,* D. Jakubczyk, M. Woźniak,* J. Archer, and M. Kolwas

Institute of Physics, Polish Academy of Sciences, Al. Lotników 32/46, 02-668 Warsaw, Poland

ABSTRACT: Models describing evaporation or condensation of a droplet have existed for over a century, and the temporal evolutions of droplet radius and temperature could be predicted. However, the accuracy of results was questionable, since the models contain free parameters and the means of accurate calibration were not available. In previous work (Hołyst et al. *Soft Matter* **2013**, *9*, 7766), a model with an efficacious parametrization in terms of the mean free path was proposed and calibrated with molecular dynamics numerical experiment. It was shown that it is essentially possible to determine reliably the temperature of a steadily evaporating/condensing homogeneous droplet relative to ambient temperature when the evolution of the droplet radius is known. The accuracy of such measurement can reach fractions of mK. In the case of an evaporating droplet of pure liquid, the (droplet) temperature is constant during the stationary stage of evaporation. In this paper, we show that, in many cases, it is also possible to determine the temporal evolution of droplet temperature from the evolution of the droplet radius if the droplet (initial) composition is known. We found the droplet radius evolution with high accuracy and obtained the evolution of droplet temperature (and composition) for droplets of (i) a two-component mixture of pure liquids; (ii) solutions of solid in liquid, one that is non-surface-active and another that is; and (iii) suspensions of non-light-absorbing and light-absorbing particles.

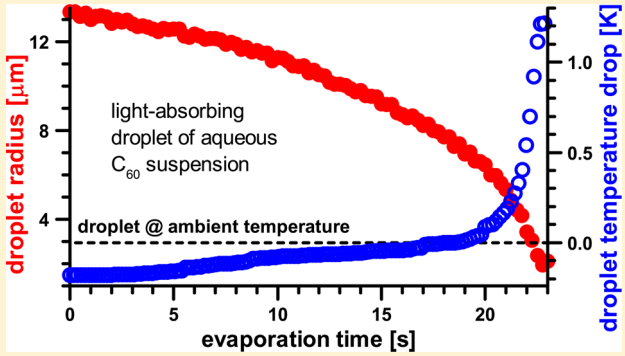

1. INTRODUCTION

The temperature of an evaporating/condensing droplet is an obviously relevant parameter in fundamental considerations as well as in technical applications. However, the difficulties in measuring it match its significance, especially for micro- and nanosize droplets and the droplets of solutions and suspensions. Several techniques, both contact and noncontact, were developed for measuring temperatures of droplets. Most of the contact (direct) methods, like suspending a droplet from a thermocouple, suffer from distorting the heat transfer, have the tendency of contaminating the droplet, and are limited by the size of the probe.[1,2] The noncontact methods are mostly based on phenomena associated with the interaction of light with matter. They often require the introduction of chemical tracers to the droplet volume[3] (and the references therein) and, for many applications, are not precise enough. Despite the large variety of methods of measurement, accuracy does not usually exceed ±1 K.

Electronic, contact methods of temperature measurement are usually categorized into four common temperature transducers: thermocouples, resistance-temperature detectors (RTDs), (semiconductor) thermistors, and integrated circuit sensors.[4] As far as the measurement of the droplet temperature is concerned, the size of the transducer is an obvious priority. This practically limits the choice to thermocouples. However, thermocouples are burdened with relatively low accuracy. On the contrary, platinum RTDs are the most accurate of the considered transducers but are significantly fragile and larger and require an external excitation current[5] which inevitably causes joule heating within the RTD, changing its temperature, and hence practically precludes its application to small droplets. The semiconductor sensors (thermistors and ICs) also require excitation current and calibration which makes them more susceptible to self-heating and permanent decalibration at extreme temperatures than RTDs or thermocouples.

Out of the noncontact methods, laser-induced fluorescence (LIF)-based diagnostics[6] is one of the widely used techniques for determination of the droplet temperature. In LIF techniques, an organic dye or a thermographic phosphor[7] chosen for the high sensitivity of its emission to the temperature is added to the liquid. This technique is partly disturbed by the tracer concentration and surface scattering on the grains of powder, respectively. Laser-induced exciplex fluorescence[8−10] has also been reported as a means to probe droplet temperature based on the ratio of excimer/monomer fluorescence intensities. However, the overlap of the fluorescence spectra of the two phases makes it difficult to distinguish them. Further on, measurement sensitivity is low at low temperature ranges and the dependence of the intensity ratio on the concentration of the dopant is a particular issue for measurement. An alternative technique to intensity-based methods is lifetime-based methods. Lifetime measurements of

Received: September 1, 2014
Revised: October 3, 2014
Published: October 7, 2014

fluorescence and phosphorescence inherently do not require the same care as intensity-based methods. The decay time can be determined using both time and frequency-domain methods. However, time-resolved measurements are instrumentally sophisticated, as they require fast detection systems and light pulses whose durations are short in comparison with the excited state lifetime.

Other measurement techniques rely on elastic or inelastic light scattering by the droplets or by the molecules of certain chemical species present in the droplet. In elastic light scattering (for example, rainbow refractometry[11]), the wavelength is not changed by scattering. In the size range of the droplets encountered in most applications, this phenomenon is rigorously described by the Mie theory.[12] Characteristic features of the light scattered by the droplets, in particular the angular position of the rainbow pattern, are very sensitive to the refractive index and thus the temperature and composition of the droplet. It is, however, very difficult to distinguish the contribution of temperature and composition variations on the refractive index.

Raman scattering[13−15] is a form of inelastic scattering on molecules which can be exploited to characterize the chemical composition of a medium and, in some cases, its temperature by using both the surface area and the position of the peaks in the Raman spectrum. The main drawback of this method is the weakness of the signal, which would in practice require high power lasers being used. Furthermore, the precision of the method ($\sim \pm 2$ K) is, for many applications, not sufficient.

Recent works based on molecular dynamics (MD) simulations[16−20] have shown that it is possible to calibrate an evaporation/condensation model against the results of MD numerical experiment. In this way, a reliable tool for determining the internal temperature (and in some cases the composition) of an evaporating/condensing droplet can be constructed. As the precision of determination of droplet temperature change reaches fractions of mK, the accuracy of droplet temperature measurement can be pushed to the limit set by ambient temperature measurement. In view of experimental uncertainties and difficulties recounted above, such a method seems to be promising. The method was demonstrated for evaporating droplets of pure liquids for which the temperature is constant during the stationary stage of evaporation. In this work, we extend the previous efforts in precise determination of microdroplet temperature to cases of mixed-liquid droplets and nonhomogeneous droplets, where temporal evolution of droplet temperature and composition is encountered. We present droplet temperature measurements for a few cases of stationary evaporation close to standard temperature and pressure (STP) conditions: (i) a two-component mixture of pure liquids, (ii) two solutions of solid in liquid: a non-surface-active and a surface-active one, and (iii) three suspensions: two non-light-absorbing (SiO_2 in water and in glycol) and the light-absorbing (C_{60} in water). In all of these cases, the droplet temperature change was below 2 K.

2. THE OUTLINE OF THE MODEL USED

A droplet evaporates at the expense of heat which is drawn both from the droplet itself and (if possible) from the ambient gas. In consequence, a temperature gradient arises toward the droplet. Classically, describing the steady evaporation (condensation) of a droplet has been based on considering the transport of mass and heat.[21,22] For large droplets close to normal conditions, both of these processes are adequately described with diffusion-type equations leading to the, so-called, "radius-square law" (compare, e.g., ref 23). However, it has been long known[24] that setting temperature continuity at the interface is not fully justified. In a microscopic picture, only the hottest molecules leave the droplet, which leads to a "temperature jump" at the interface (compare: evaporative cooling in atomic physics). The discontinuity of the temperature profile at the interface was ultimately shown in the elegant experiment of Fang and Ward.[25] However, the description of temperature (and density) profiles in the vicinity of the interface encounters persisting difficulties (compare refs 26 and 27). In the limiting case, when the mean free path is comparable to the extent of the interface (e.g., close to critical conditions), the description with hydrodynamic equations seems sufficient.[28] In the opposite limiting case, when the mean free path is much larger than the extent of the interface (droplet evaporating into a vacuum), the kinetic theory of gases and the Hertz−Knudsen−Langmuir (HKL) equation are evoked to describe the ballistic transport. Unexpectedly, describing the transport of mass and heat across the interface with the kinetic theory of gases encounters difficulty in itself and seems to require a phenomenological parameter—the coefficient of accommodation[29] (aka the evaporation/condensation coefficient). This parameter turned out to be extremely difficult to measure (compare, e.g., ref 18). Further on, the hydrodynamic and kinetic descriptions cannot be easily reconciled, leading to further parameters (see, e.g., refs 30−32). The classical approach to reconciling the diffusive and ballistic transport leads to the differential equation describing droplet radius evolution $a(t)$ in a general form (see refs 18 and 17 for derivation at the micro- and nanoscale, respectively):

$$\dot{a} = \frac{P_1}{a/(1 + P_3/a) + P_2} \tag{1}$$

where $P_{1,2,3}$ compound parameters (see below) are not in general constant. In classical parametrization, P_3 is rather vague (compare eqs 13 and 14 and 13−20 in ref 30), which also blurs the value of P_2.

However, the analysis of MD experiments performed in ref 16 showed that the temperature discontinuity at the interface can be conveniently parametrized in terms of the mean free path (see eq 11 therein). The parametrization retains the well-known functional dependence but is unambiguous and simple. Furthermore, it uses the temperature of the droplet interior rather than the temperature of vapor near the droplet surface (as could be found in classical works). For a single-component, homogeneous droplet, the transport equations take then the form

$$\dot{a} = \frac{P_k}{a + Al_{\mathrm{mfp}}} \tag{2}$$

where $k = m, t$, with

$$P_{\mathrm{m}} = \frac{DM}{R\rho_{\mathrm{L}}}\left[\frac{Sp_{\mathrm{sat}}(T_\infty)}{T_\infty} - \frac{p_{\mathrm{a}}(T_{\mathrm{L}})}{T_{\mathrm{L}}}\right] \tag{3}$$

when the transport of mass is considered, and

$$P_{\mathrm{t}} = \frac{\lambda \Delta T}{q\rho_{\mathrm{L}}}, \quad \text{where } \Delta T = T_{\mathrm{L}} - T_\infty \tag{4}$$

when the transport of heat from the ambient atmosphere (non-light-absorbing droplets) is considered. M, ρ_{L}, and q are the

dx.doi.org/10.1021/jp508823z | J. Phys. Chem. B 2014, 118, 12566−12574

molecular mass, the liquid density, and the (effective) enthalpy of evaporation of the evaporating component. D is the evaporating component diffusion coefficient in the surrounding gaseous medium, and p_{sat}, p_a, and S are its saturated vapor pressure, its equilibrium vapor pressure over the droplet surface, and its relative saturation far from the droplet, respectively. λ and l_{mfp} are the thermal conductivity coefficient and the mean free path of the surrounding gaseous medium, and R is the universal gas constant. T_∞ and T_L are the temperature far from the droplet and the temperature of the droplet, respectively. It was shown in ref 16 that T_L has a well-defined physical meaning of internal droplet temperature and A = 2.35. In extreme cases, when a significant internal temperature gradient is present, the temperature just below the surface can be used for parametrization. The equilibrium vapor pressure above the droplet surface is expressed by the Kelvin equation (see, e.g, eq 9.17 in ref 33)

$$p_a(T_L) = p_{sat}(T_L)\exp\left(\frac{M}{RT_L\rho_L}\frac{2\gamma}{a}\right) \quad (5)$$

where γ is the surface tension of the liquid. For micron-sized droplets, the surface tension effect is negligible in comparison to modification of p_{sat} due to the temperature drop from T_∞ to T_L. The surface tension effect must be however considered at the sub-microscale (see ref 17). Similarly, the effect of the droplet electrical charge (see, e.g., eq 29 in ref 33) is negligible at the microscale but should be considered at the nanoscale. $P_t \equiv P_m$ as long as eq 2 (in its basic form) holds. For a homogeneous, single-component droplet, P_k is very nearly constant. Equations 2, 3, and 4 are the starting point for considering the steady evolution of more complex micro- or even nanodroplets (mixed liquid, solution, or suspension).

2.1. Circumventing the Ill-Conditioning of the Problem. In principle, equation(s) 2 enable predicting the droplet radius and temperature evolution *a priori*. However, in frequently encountered cases, when P_k expresses a small difference between large quantities, the equation(s) become ill-conditioned. Such is the case for slowly evaporating liquids, where $T_L \simeq T_\infty$ (e.g., in the case of glycerol, $\Delta T/T_\infty \simeq 10^{-6}$). Similarly, for high S ($\gtrsim$0.7, e.g., in a humid atmosphere), $p_a \simeq p_{sat}$. This imposes upon parameters S and T_∞ a requirement of experimentally unattainable accuracy.

However, ΔT and $(Sp_{sat} - p_a)$ can be determined with high accuracy *a posteriori* from the observed droplet radius evolution. The adopted procedure depends on the considered case and the quality of experimentally obtained $a(t)$ data. There are two general courses that can be taken. They are valid also for the composite droplets. (i) If the experimental $a(t)$ is smooth and can be reliably differentiated, eq 2 can be used in differential form either for direct calculation or for fitting (e.g., $1/\dot{a}(a)$ has a linear form convenient for fitting). (ii) If experimental $a(t)$ is noisy, eq 2 must be integrated first: analytically or numerically (with awareness of the effects of ill-conditioning) and then used for direct calculation or for fitting. This course must also be taken when P_k cannot be treated as constant, for example, for very large $|\Delta T|$.

In ref 16, T_L = const was found for single-component droplets of clear liquids. In the present work, we demonstrate that, when a droplet temperature evolution occurs, it is unambiguously bound with the droplet radius and composition evolution. Thus, $T_L(t)$ can be retrieved from $a(t)$ if the droplet (initial) composition is known. The adopted procedures are described in detail in sections 4−6.

3. EXPERIMENTAL SETUP AND SAMPLE PREPARATION

3.1. Trapping of Droplets. All our experiments on droplet evaporation were conducted on single, electrically charged droplets levitated in an electrodynamic trap in a stationary atmosphere. Electrodynamic trapping with a combination of AC and DC electric fields is a fairly well developed technique, which enables constraining charged particle(s) to a very small volume (<1 μm^3) (see, e.g., refs 34 and 35). The principle of electrodynamic trapping allows wide variations of the trap design (compare refs 15 and 36−41). In our lab, we also designed a line of traps suiting our needs.[42−44] For introducing droplets into the trap, we used a droplet-on-demand injector. We designed and used a line of various injectors.[16,43,45] Droplets get charged by charge separation (due to charge fluctuations or in applied field) on emerging from the injector nozzle. The trap was kept in a small (~10 cm^3) climatic chamber with stabilized temperature (±0.15 K) and composition of atmosphere (see below).

3.2. Droplet Radius Determination. The outline of our experimental procedure is presented in Figure 1. The relative

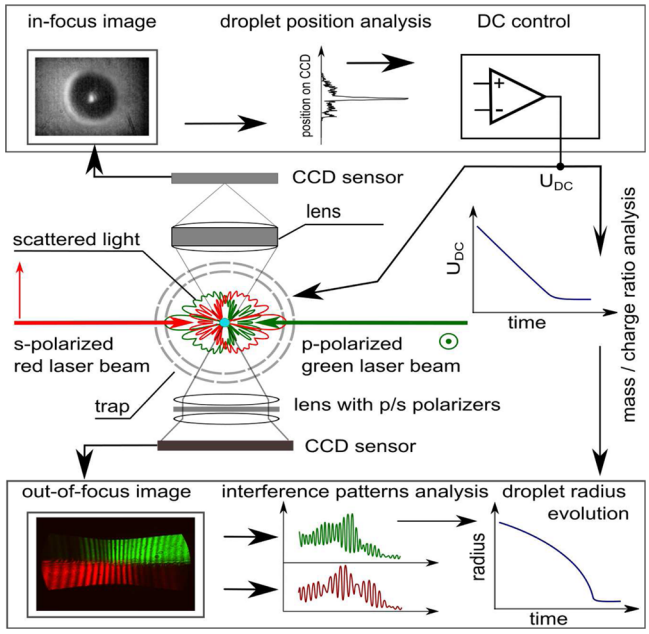

Figure 1. Outline of the experimental setup and procedures. A four-ring electrodynamic trap was used. Scattered light was collected around right angles to the illumination direction. The trap was equipped with a droplet vertical position stabilization loop which enabled droplet weighting by following the DC voltage.

droplet temperature measurements presented in this study are based on the analysis of temporal evolution of droplet radius. The droplet radius was determined (simultaneously) in two ways: with static light scattering analysis (optical particle characterization) and with droplet weighting with the DC field. Below, we give the outline of the method, while further details can be found in ref 46.

Two coaxial, counter propagating laser beams of ~10 mW power each (inside the trap) and ~0.5 mm waist were used simultaneously for droplet illumination: green (532 nm) p-

dx.doi.org/10.1021/jp508823z | J. Phys. Chem. B 2014, 118, 12566−12574

polarized (horizontal) and red (654 nm) s-polarized (vertical). The droplet was in the focus of a lens with NA = 0.28, and the scattered light was collected around the right angle in the horizontal scattering plane. This entirely defocused image of the droplet (see the out-of-focus image in Figure 1) was used for scatterometry. The distortions of frequency and shape of the interference fringes (spherical aberration and other geometrical effects) were corrected numerically in postprocessing. Simultaneously, the focused image of the droplet (see the in-focus image in Figure 1) was used for droplet position stabilization. The vertical position of the (evaporating) droplet was maintained at the trap center with a PID type stabilizing loop, applying a balancing DC voltage between the top and bottom electrode. No secular (macro) motion was observed. In lateral directions, the droplets performed only trapping-potential-constrained Brownian motions. Brownian rotations were also plainly visible in the case of inhomogeneous droplets. Neither photophoresis nor thermophoresis nor radiation pressure effects were observed.

In the case of pure liquid, we used the Mie scattering lookup table method (MSLTM). MSLTM bases on fitting (with gradientless, lookup table method) the complete Mie theory predictions to the experimentally obtained scattering patterns. In favorable cases (slowly evaporating liquids, refractive index known *a priori*), the method yields a droplet radius with an accuracy up to ±10 nm. For droplets of mixed liquid, we used MSLTM with the evolution of the refractive index iteratively accounted for with the Weiner formula, while the droplet composition evolution was sought with the evaporation model (see section 4). The refractive index and its dispersion curve for water were taken from ref 47. For glycerine and diethylene glycol (organic solvents), the n_{D20} refractive indices were taken from the lot specifications provided by manufacturers, while the dispersion curves were adapted from refs 48 and 49. For SiO_2 nanospheres and C_{60} nanocrystallites, we adapted data from refs 50 and 51, respectively.

In the case of droplets with inclusions, we used the angular frequency of scattered light method (AFSLM). AFSLM bases on the general observation that the characteristic angular frequency of the scattering pattern for s polarization is approximately proportional to the droplet radius. For observation around the right angle, AFSLM can be treated as insensitive to the scattering particle refractive index. The characteristic frequency was conveniently obtained with FFT of angular irradiance distribution (compare refs 52−54). AFSLM yields a droplet radius with ±100 nm accuracy only but is much more resistant to interference fringe distortion than MSLTM. The radius determination accuracy could then be further improved by simultaneous weighting of the droplet. Weighting in an electrodynamic trap bases on balancing the charged droplet weight with the electrostatic field. The accuracy of droplet radius determination based on weighting reaches, in favorable cases, ±30 nm.

3.3. Droplet Material Preparation. We used three types of liquids: (i) diethylene glycol (DEG; 99.99 GC area %, BioUltra, Fluka), (ii) glycerol 99.5% (anhydrous pure p.a., Chempur), and (iii) ultrapure water (produced in the lab with Milli-Q Plus, Millipore, total dissolved solids <20 ppb). In a glycerol/DEG mixture, the initial mass fraction of glycerol was 0.2.

The sodium dodecyl sulfate (SDS; Sigma-Aldrich, ACS Reagent, ≥99.0%) solution in DEG was 2 mg/mL. The suspensions of 225 nm radius SiO_2 microspheres (C-SIO-0.45, Corpuscular) in DEG also contained a significant amount of SDS. The material was prepared by first mixing SDS/DEG solution with an aqueous suspension of SiO_2 nanospheres. After the injection of a microdroplet into the dry nitrogen atmosphere (see below), the water fraction evaporates in a fraction of the first second (compare refs 44 and 55), leaving SiO_2 microspheres and SDS in DEG. The final proportion of (SiO_2 + SDS)/DEG was (3 mg + 2 mg)/mL.

The aqueous suspension of fullerene nanocrystallites (~8 nm mean diameter, see Figure 2 in ref 56) was prepared by sonicating fullerene powder (99% C_{60}, MER) in ultrapure water and filtering shortly before the experiment (~15 μm pore size filtering paper and 450 nm pore size filter (SM11306, Sartorius)). The initial suspension concentration was ~3 μg/mL. All liquids were transferred into the droplet injector with due care and without delay. The experiment was conducted within 1 h after the transfer.

3.4. Experimental and Modeling Conditions and Parameters. We used two types of atmosphere in the chamber: (1) dry nitrogen for DEG-based droplets and (2) nitrogen with water vapor for water-based droplets. The humidity was nearly maximal then (saturated vapor), and it was tentatively measured (±3%) with the semiconductor sensor (HIH3610-2, Honeywell). The pressure in the chamber was atmospheric, and its natural variations had no effect upon the studied phenomena.

Molecular masses, densities, and enthalpies of vaporization used in modeling were taken from refs 57, 58, and 59. The coefficients of diffusion of vapor in air were taken from refs 60 (DEG), 61 (glycerol), and 57 (water). The temperature dependence of diffusion coefficients was adapted from ref 60. The temperature dependence of vapor pressure (Antoine equation), which is crucial for the reliable modeling, was taken from refs 62 (DEG), 63 (glycerol), and 58 (water). The T_∞, S, and n_s (see section 5) thermodynamic conditions of presented experiments with solutions/suspensions of solids are listed in Table 1.

Table 1. T_∞, S, and n_s Thermodynamic Conditions of Presented Experiments[a]

droplet material	S	S_{Fit}	T_∞	n_s
H_2O + $(NH_4)_2SO_4$	0.8	0.835	25.0	6.2×10^{-3}
H_2O + SiO_2 nanospheres	0.9	0.944	15.2	4.4×10^{-4}
H_2O + C_{60} nanocrystallites	0.95	0.983	15.0	3×10^{-4}
DEG + SDS	0	0	24.3	2.9×10^{-3}
DEG + SiO_2 nanospheres	0	0	26.5	3.64×10^{-2}

[a] S was measured with a semiconductor sensor for aqueous suspensions, was assumed zero (dry conditions) for DEG solution and suspension, and was taken from ref 64 for $(NH_4)_2SO_4$ aqueous solution. n_s is proportional to the initial mass fraction (see section 5 for details). S_{Fit} and n_s values found from optimization for all cases.

4. TEMPERATURE OF EVAPORATING DROPLET OF A MIXTURE OF PURE NON-LIGHT-ABSORBING LIQUIDS

It can be noticed that, for a mixture of pure non-light-absorbing liquids, the droplet temperature reflects the changes of mass transport caused by the evolution of composition. The transport equations take then a more general form, including Raoult's law:

$$\frac{\rho_{L_i}}{3a^2}\frac{\mathrm{d}}{\mathrm{d}t}(a^3 Y_i) = \frac{D_i M_i}{R(a + Al_{\mathrm{mfp}})}\left[\frac{S_i p_{\mathrm{sat}_i}(T_\infty)}{T_\infty} - \frac{p_{a_i}(T_\mathrm{L})}{T_\mathrm{L}} X_i\right] \tag{6}$$

$$\frac{1}{3a^2}\frac{\mathrm{d}}{\mathrm{d}t}\left(\sum_i a^3 Y_i \rho_{L_i} q_i\right) = \frac{\lambda \Delta T}{a + Al_{\mathrm{mfp}}} \tag{7}$$

where subscript i indexes the component and X_i and Y_i are the component mole and volume fraction, respectively. We assume additivity of constituent volumes (compare the Weiner formula), so the mole and volume fractions can be expressed by one another as follows

$$X_i = \frac{Y_i/V_{mi}}{\sum_i Y_i/V_{mi}} \tag{8}$$

where V_{mi} is the molar volume of the ith component.

We illustrate the case with the evolution of a droplet of DEG/glycerol mixture (Figure 2). In this case, $|\Delta T|$ is (expected to be) very small. We apply and discuss both procedures of temperature evolution determination mentioned in section 2.1.

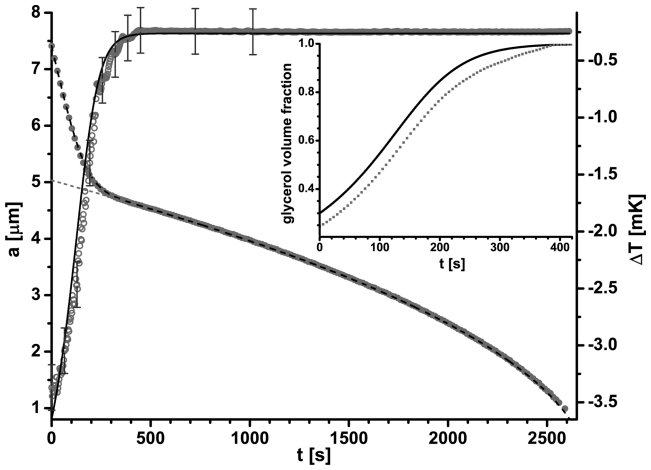

Figure 2. Temporal evolution of droplet radius $a(t)$ (solid circles merged into a line) and of relative temperature $\Delta T(t)$ (open circles and solid line) for a droplet of 1:5 glycerol/DEG mixture evaporating into a nitrogen atmosphere, at STP conditions. Open circles represent direct calculation with eq 7 (method i). The solid line represents numerical integration of equations and fitting them to experimental data (method ii). The uncertainty of droplet radius and of relative temperature for method ii is smaller than the marker size, while the uncertainty of relative temperature for method i is shown with error bars. The evolution of droplet composition (glycerol volume fraction) is shown in the inset (solid squares).

(i) It can be seen in Figure 2 that $a(t)$ is fairly smooth and $\dot{a}(a)$ can be calculated. Thus, ΔT could be easily retrieved from the experimental $a(t)$ by means of the heat transport equation (eq 7), if only the evolution of volume fraction $Y_i(t)$ (droplet composition) was known. An estimate of the volume fraction evolution can be found from the changes of refractive index of the droplet at the stage of radius finding (Weiner formula, see section 3). As the first approximation, this can be done by assuming that the presence of the more volatile fraction (DEG) does not influence the evaporation of the less volatile fraction (glycerol, see dashed (red) line in Figure 2).

The approximate glycerol volume fraction is shown as a dotted (gray) line in the inset in Figure 2. The corresponding ΔT found directly from eq 7 is represented in Figure 2 with open (gray) circles. The procedure is rather simple, but minute errors of the radius retrieval method are magnified by differentiation and require postfiltering. The uncertainty of ΔT (shown with the error bars) is dominated by these errors.

(ii) The temporal evolution $\Delta T(t)$ can also be determined by straightforward numerical integration of the set of eqs 6 and 7 and fitting the solution to experimental $a(t)$. Since in the considered case $S = 0$, $Y_1(0)$ (initial volume fraction) is the only parameter of the fit. The problem is well-conditioned versus $Y_i(t)$, so the obtained $\Delta T(t)$ is also reliable. The glycerol volume fraction obtained in this way is presented in the inset in Figure 2. The corresponding $a(t)$ and $\Delta T(t)$ resulting from the model are presented as dashed and solid lines in Figure 2.

5. TEMPERATURE OF EVAPORATING DROPLET OF NON-LIGHT-ABSORBING SOLUTION AND SUSPENSION

Procedure i described above could be, in principle, used in the case of non-light-absorbing solution and suspension. Since dissolved or dispersed solid does not evaporate, eq 7 would be simplified. However, the presence of a dissolved or dispersed phase compromises the accuracy of radius measurement and $\dot{a}(t)$ becomes excessively noisy. It can be smoothed in postprocessing, but better results are obtained with procedure ii when the full model is fitted to the experimental data.

In that case, P_k is also not constant and the mass transport equation must be suitably modified. We found it sufficient that the exponential Köhler term (compare refs 30 and 33) is introduced into the P_m parameter in the following manner:

$$P_\mathrm{m} = \frac{DM}{R\rho_\mathrm{L}}\left\{\frac{S p_{\mathrm{sat}}(T_\infty)}{T_\infty} - \frac{p_\mathrm{a}(T_\mathrm{L})}{T_\mathrm{L}} \exp\left[\frac{-n_\mathrm{s}}{(a/a_0)^3 - n_\mathrm{s}}\right]\right\} \tag{9}$$

where a_0 is the initial droplet radius and n_s plays the role of the parameter in the Köhler equation (see, e.g., eq 6-27 in ref 30). It is proportional to the initial mass fraction.

Thus, in order to retrieve $\Delta T(t)$, the set of eqs 2 with 4 and 9 must be integrated numerically and fitted to the experimental $a(t)$. The problem is ill-conditioned in terms of the parameter S, and the accuracy of S measurement (see section 3) is fundamentally too low. In consequence, both S and n_s must be fitted. This is feasible as long as S is constant throughout the whole evolution. We verified that the fit is unambiguous (see Figure 5) and may serve for determination of S with accuracy better than provided by measurement with the sensor. However, it must be kept in mind that the full precision of S obtained by fitting has no direct physical meaning (see section 2.1).

We verified the procedure using independent data for $(NH_4)_2SO_4$ solution published in ref 64. Using model equations, we reconstructed the radius evolution and S value and thus obtained the droplet temperature evolution as well (Figure 3, top). Then, we applied the procedure to our own experimental data: surface-active compound solution (SDS in DEG, Figure 3, bottom) and non-light-absorbing coarse suspension (SiO_2 nanospheres in DEG + SDS and in water, Figure 4). It is worth noticing that when the procedure is applied to good quality $a(t)$ data (as in Figure 3, bottom) the uncertainty of the resulting $\Delta T(t)$ is also very small.

dx.doi.org/10.1021/jp508823z | J. Phys. Chem. B 2014, 118, 12566−12574

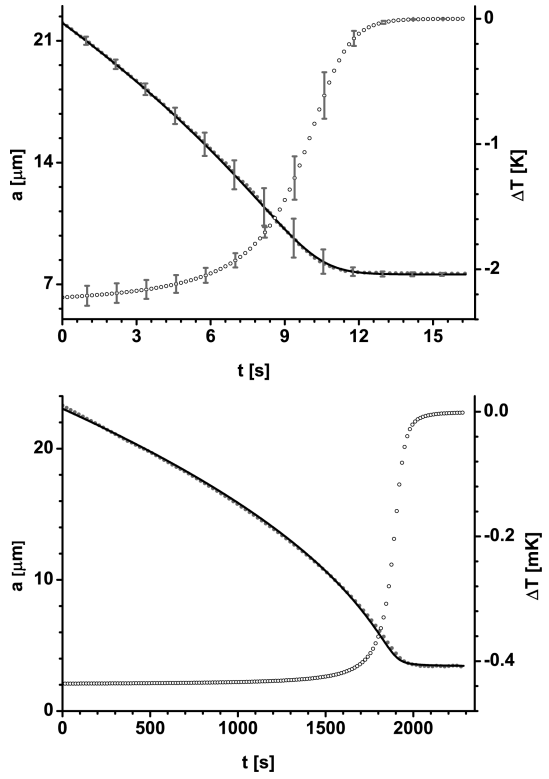

Figure 3. Top panel: the temporal evolution of droplet radius $a(t)$ (gray, solid circles), as published in ref 64 for a droplet of $(NH_4)_2SO_4$ (0.15 M) aqueous solution evaporating into humid air ($S \simeq 0.8$). This evolution was reproduced by integrating the set of eqs 2, 4, and 9 numerically (black, solid line) for T_∞ = 298.15 K, ambient pressure of 101.325 kPa, S = 0.835, and $n_s = 6.2 \times 10^{-3}$. The procedure yielded also the corresponding evolution of relative temperature $\Delta T(t)$ (open circles). The error bars correspond to experimental uncertainties reported in ref 64. Bottom panel: the temporal evolution of droplet radius $a(t)$ (gray, solid circles) for a droplet of solution of SDS (surface active agent) in DEG. Model equations fit to $a(t)$ data are represented with the black, solid line. The corresponding relative temperature evolution $\Delta T(t)$ found from fitting is represented with open circles. The uncertainties of radius measurement and of relative temperature are smaller than marker sizes.

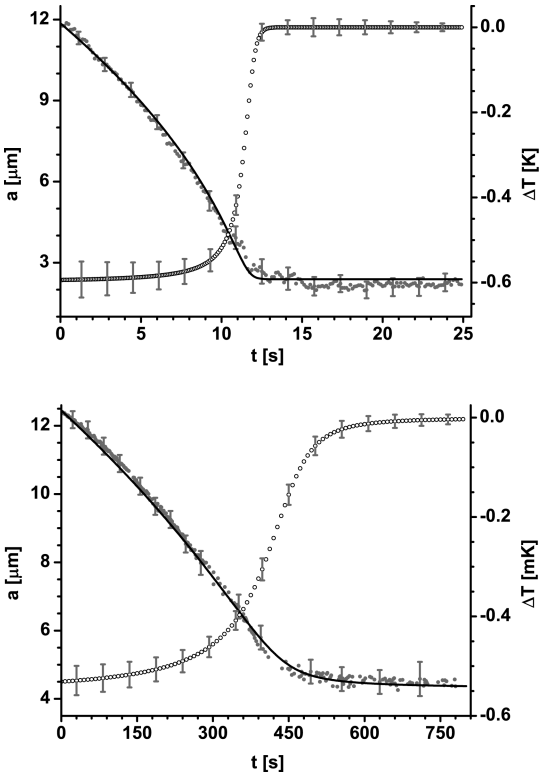

Figure 4. Temporal evolution of droplet radius $a(t)$ (gray, solid circles) and the model equations fit to $a(t)$ data (black, solid line) for a droplet of (top panel) a suspension of SiO_2 225 nm radius nanospheres in SDS/DEG solution and (bottom panel) an aqueous suspension of SiO_2 225 nm radius nanospheres. The corresponding relative droplet temperature $\Delta T(t)$ found from fitting is represented with open circles. The estimated uncertainties of radius measurement and relative temperature are shown with error bars.

In all cases presented in Figures 3 and 4, the evaporation finally stopped and so the final ΔT = 0. We found that our result for the SDS in DEG solution is in line with the result for SDS in water reported in ref 64 (Figures 9 and 10 therein). This finding confirms that for micron sized droplets there is no measurable effect of surface activity on the evaporation rate.

6. TEMPERATURE OF EVAPORATING DROPLET OF LIGHT-ABSORBING SUSPENSION

Procedure ii based on numerically solving transport equations (forward modeling of evolution) can also be successfully applied to cases of droplets of light-absorbing suspension. The mass transport equation, as previously, comprises the Köhler term, while the heat transport equation must account for the presence of internal heat source(s) (light absorption). In general, some external data might be required. We illustrate the case with the evaporation of a light-absorbing droplet of fine aqueous dispersion of C_{60} fullerene nanocrystallites evaporating into a humid atmosphere.

In our experiment with absorbing droplets, the absorption of light was very low at the beginning of droplet evolution and in the process of evaporation it was rising. However, during the whole evolution that we studied in the present work, the photophoretic effects did not manifest. The radiant flux absorbed by an evaporating droplet could be found as $I_0 \cdot C_{abs}$, where I_0 is the incident light irradiance and the absorption cross section C_{abs} was calculated with the aid of Mie theory (see, e.g., ref 12). The changes of the imaginary part of the refractive index of suspension $\mathfrak{I}(m)$, which follow the changes of composition due to evaporation, must also be accounted for (see the inset in Figure 6). We could express $\mathfrak{I}(m(t))$ with the aid of the n_s parameter.

The Mie theory can provide the distribution of energy inside a homogeneous light-absorbing droplet. However, the analysis of movement of speckles visible in light scattered by the (light-absorbing) droplet with inclusions showed that the droplet was rotating (tumbling) randomly at all stages of evolution due to Brownian forces (see section 3). It can be expected that due to random rotations the droplet volume is heated uniformly (distribution of droplet temperature is uniform). On the other hand, the model of evaporation that we utilized actually binds the droplet radius evolution with the temperature just below the droplet surface and ignores possible internal temperature gradients. It must be kept in mind that in the case that we considered the temperature rise was of the order of only a few Kelvins and the possible radial temperature gradients of less than 1 K could not be possibly measured with existing remote sensing methods (like Raman spectroscopy).

dx.doi.org/10.1021/jp508823z | J. Phys. Chem. B 2014, 118, 12566−12574

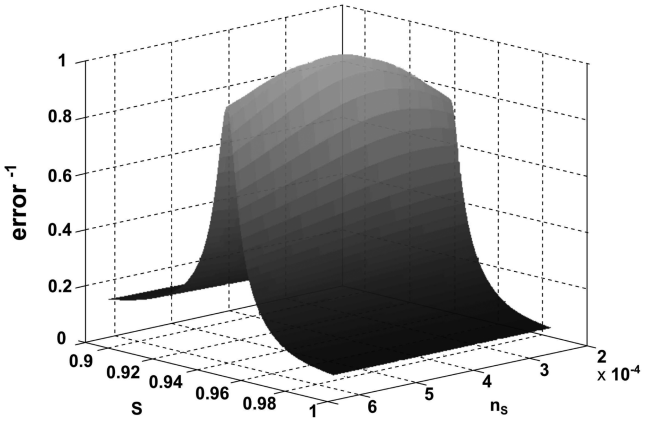

Figure 5. Quality of fitting the set of eqs 2, 4, and 9 to $a(t)$ experimental data corresponding to Figure 3: error = $(\sum_i^N[a_{exp}(t_n) - a_{theor}(t_n)]^2)^{1/2}$, where t_n are experimental time points and N is the length of the movie.

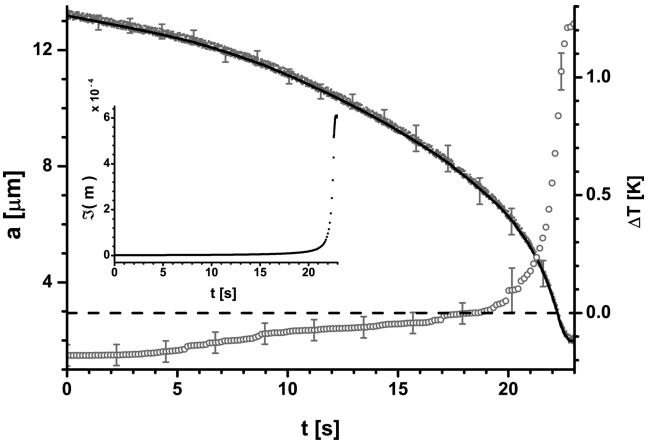

Figure 6. Temporal evolution of droplet radius $a(t)$ (gray, solid circles) and the model equations fit to $a(t)$ data (black, solid line) for a droplet of aqueous C_{60} fullerene suspension. The corresponding relative droplet temperature $\Delta T(t)$ found from fitting is represented with open circles. The estimated uncertainty of radius measurement and of relative temperature is shown with error bars. It is worth noticing that the droplet temperature rises above the ambient temperature; ΔT changes its sign (crosses the dashed line). The evolution of the imaginary part of the refractive index of the suspension $\Im(m(t))$ is shown in the inset.

We consider it sufficient to express P_t in the following form:

$$P_t = \frac{I_0 C_{abs}(a)/(4\pi a) - \lambda(T_\infty - T_L)}{q\rho_L} \quad (10)$$

Again, it is important for the presented method that S remains constant throughout the evolution. The model was numerically integrated and fitted to experimental $a(t)$ with S and n_s optimization. The results are presented in Figure 6. The rise of temperature due to heating by light is plainly visible. Further on, the final temperature of the droplet is visibly higher than the temperature of the chamber, though ΔT did not exceed 1.3 K.

7. CONCLUSIONS

Recent theoretical works made possible the determination of internal temperature of an evaporating/condensing droplet of pure liquid. The precision of such measurement, relative to ambient temperature, reaches fractions of mK, and the accuracy is limited by the accuracy of the ambient temperature measurement (usually ∼0.1 K). The method requires measuring the droplet radius evolution only. We extended this technique beyond the single-component droplets of clear (pure) liquids, for which the temperature is constant, and determined temporal evolution of droplet temperature for a few cases of different complexity. We analyzed mixed-liquid droplets, droplets of solution of solid, and droplets of suspension, both non-light-absorbing and light-absorbing. In the case of light-absorbing droplets, the temperature just below the surface can be determined. Together with the droplet temperature evolution, we could also determine the evolution of droplet composition. It can be noticed that the droplet temperature evolution of a composite droplet is bound to the composition evolution. In consequence, the droplet temperature can be, to some extent, programmed by engineering the droplet composition (e.g., several volatile and nonvolatile components) and absorption cross section (light-absorbing liquids and solids).

AUTHOR INFORMATION

Corresponding Authors

*E-mail: derkaczg@ifpan.edu.pl. Phone: (+48) 22 116 3277.
*E-mail: mwozniak@ifpan.edu.pl. Phone: (+48) 22 116 3277.

Notes

The authors declare no competing financial interest.

REFERENCES

(1) Harada, T.; Watanabe, H.; Suzuki, Y.; Kamata, H.; Matsushita, Y.; Aoki, H. A numerical investigation of evaporation characteristics of a fuel droplet suspended from a thermocouple. *Int. J. Heat Mass Transfer* **2011**, *54*, 649−655.
(2) McGaughey, A.; Ward, C. Temperature discontinuity at the surface of an evaporating droplet. *J. Appl. Phys.* **2002**, *91*, 6406−6415.
(3) Lemoine, F.; Castanet, G. Temperature and chemical composition of droplets by optical measurement techniques: a state-of-the-art review. *Exp. Fluids* **2013**, *54*, 1572−1606.
(4) Practical temperature measurements, Application Note 290; Agilent Technologies: 2012.
(5) Ehinger, K.; Flach, D.; Gellrich, L.; Horlebein, E.; Huck, R.; Ilgner, H.; et al. *Industrial temperature measurement. Basics and practice*; ABB Automation Products GmbH: 2013.
(6) Lakowicz, J. *Principles of fluorescence spectroscopy*; Springer: New York, 2006.
(7) Omrane, A.; Särner, G.; Engström, J.; Aldén, M. Development of temperature measurements using thermographic phosphors: Applications for combustion diagnostics. *European Combustion Meeting* **2005**, *76*, 1−6.
(8) Zhang, Y.; Zhang, G.; Xu, M.; Wang, J. Droplet temperature measurement based on 2-color laser-induced exciplex fluorescence. *Exp. Fluids* **2013**, *54*, 1583−1593.
(9) Murray, A.; Melton, L. Fluorescence methods for determination of temperature in fuel sprays. *Appl. Opt.* **1985**, *24*, 2783−2787.
(10) Parigger, C.; Plemmons, D.; Litchford, R.; Jeng, S. Exciplex liquid-phase thermometer using time-resolved laser-induced fluorescence. *Opt. Lett.* **1998**, *23*, 76−78.
(11) Saengkaew, S.; Charinpanitkul, T.; Vanisri, H.; Tanthapanichakoon, W.; Mees, L.; Gouesbet, G.; Gréhan, G. Rainbow refractrometry: On the validity domain of Airy's and Nussenzveig's theories. *Opt. Commun.* **2006**, *259*, 7−13.
(12) Bohren, C.; Huffman, D. *Absorption and Scattering of Light by Small Particles*; Wiley: New York, 1998.
(13) Schweiger, G. Raman scattering on single aerosol particles and on flowing aerosols: a review. *J. Aerosol Sci.* **1990**, *21*, 483−509.

(14) Smith, J.; Cappa, C.; Drisdell, W.; Cohen, R.; Saykally, R. Raman Thermometry Measurements of Free Evaporation from Liquid Water Droplets. *J. Am. Chem. Soc.* **2006**, *128*, 12892−12898.
(15) Heinisch, C.; Wills, J.; Reid, J.; Tschudi, T.; Tropea, C. Temperature measurement of single evaporating water droplets in a nitrogen flow using spontaneous Raman scattering. *Phys. Chem. Chem. Phys.* **2009**, *11*, 9720−9728.
(16) Hołyst, R.; Litniewski, M.; Jakubczyk, D.; Zientara, M.; Woźniak, M. Nanoscale transport of energy and mass flux during evaporation of liquid droplets into inert gas: computer simulations and experiments. *Soft Matter* **2013**, *9*, 7766−7774.
(17) Zientara, M.; Jakubczyk, D.; Litniewski, M.; Hołyst, R. Transport of Mass at the Nanoscale during Evaporation of Droplets: the Hertz-Knudsen Equation at the Nanoscale. *J. Phys. Chem. C* **2013**, *117*, 1146−1150.
(18) Hołyst, R.; Litniewski, M.; Jakubczyk, D.; Kolwas, K.; Kolwas, M.; Kowalski, K.; Migacz, S.; Palesa, S.; Zientara, M. Evaporation of freely suspended single droplets: experimental, theoretical and computational simulations. *Rep. Prog. Phys.* **2013**, *76*, 034601−034620.
(19) Cheng, S.; Lechman, J.; Plimpton, S.; Grest, G. Evaporation of Lennard-Jones fluids. *J. Chem. Phys.* **2011**, *134*, 2247041−22470413.
(20) Varilly, P.; Chandler, D. Water Evaporation: A Transition Path Sampling Study. *J. Phys. Chem. B* **2013**, *117*, 1419−1428.
(21) Maxwell, J. On stresses in rarefied gases arising from inequalities of temperature. *Philos. Trans. R. Soc. London* **1879**, *170*, 231−256.
(22) Maxwell, J. *Collected Scientific Papers* **1890**, *11*, 625.
(23) Jakubczyk, D.; Kolwas, M.; Derkachov, G.; Kolwas, K.; Zientara, M. Evaporation of Micro-Droplets: the "Radius-Square-Law" Revisited. *Acta Phys. Pol., A* **2012**, *122*, 709−716.
(24) Langmuir, I. The Dissociation Of Hydrogen Into Atoms. [Part II.] Calculation Of The Degree Of Dissociation And The Heat Of Formation. *J. Am. Chem. Soc.* **1915**, *37*, 417−458.
(25) Fang, G.; Ward, C. Temperature measured close to the interface of an evaporating liquid. *Phys. Rev. E* **1999**, *59*, 417−428.
(26) Fang, G.; Ward, C. Examination of the statistical rate theory expression for liquid evaporation rates. *Phys. Rev. E* **1999**, *59*, 441−453.
(27) Hołyst, R.; Litniewski, M. Heat Transfer at the Nanoscale: Evaporation of Nanodroplets. *Phys. Rev. Lett.* **2008**, *100*, 055701−1−4.
(28) Babin, V.; Hołyst, R. Evaporation of a Sub-Micrometer Droplet. *J. Phys. Chem. B* **2005**, *109*, 11367−11372.
(29) Knudsen, M. *The Kinetic Theory of Gases: Some Modern Aspects*; Methuen: London, 1950.
(30) Pruppacher, H.; Klett, J. *Microphysics of Clouds and Precipitation*; Kluwer: Dordrecht, The Netherlands, 1997.
(31) Sirignano, W. *Fluid Dynamics and Transport of Droplets and Sprays*; Cambridge University Press: Cambridge, U.K., 2010.
(32) Sazhin, S. Modelling of heating, evaporation and ignition of fuel droplets: combined analytical, asymptotic and numerical analysis. *J. Phys.: Conf. Ser.* **2005**, *22*, 174−193.
(33) Friedlander, S. *Smoke, Dust and Haze Fundamentals of Aerosol Dynamics*; Oxford University Press: New York, Oxford, U.K., 2000.
(34) Paul, W. Electromagnetic traps for charged and neutral particles. *Rev. Mod. Phys.* **1990**, *62*, 531−540.
(35) Major, F.; Gheorghe, V.; Werth, G. *Charged Particle Traps*; Springer: Berlin, 2005.
(36) Davis, E.; Buehler, M.; Ward, T. The double-ring electrodynamic balance for microparticle characterization. *Rev. Sci. Instrum.* **1990**, *61*, 1281−1288.
(37) Arnold, S. A three-axis spherical void electrodynamic levitator trap for microparticle experiments. *Rev. Sci. Instrum.* **1991**, *62*, 3025−3028.
(38) Shaw, R.; Lamb, D. Experimental determination of the thermal accommodation and condensation coefficients of water. *J. Chem. Phys.* **1999**, *111*, 10659−10663.
(39) Allison, E.; Kendall, B. Cubic electrodynamic levitation trap with transparent electrodes. *Rev. Sci. Instrum.* **1996**, *67*, 3806−3812.
(40) Itoh, M.; Arakawa, E.; Sakiyama, K.; Tanaka, K.; Takano, H. Manipulation of a single aerosol particle in a quadrupole cell by dual-sided invisible laser irradiation. *J. Aerosol Sci.* **1999**, *30*, S403−S404.
(41) Davies, J.; Haddrell, A.; Reid, J. Time-Resolved Measurements of the Evaporation of Volatile Components from Single Aerosol Droplets. *Aerosol Sci. Technol.* **2012**, *46*, 666−677.
(42) Markowicz, P.; Jakubczyk, D.; Kolwas, K.; Kolwas, M. Trapping of light-induced sodium clusters in a modified quadrupole trap. *J. Phys. B* **2000**, *33*, 3605−3614.
(43) Jakubczyk, D.; Zientara, M.; Bazhan, W.; Kolwas, M.; Kolwas, K. A device for light scatterometry on single levitated droplets. *Opto-Electron. Rev.* **2001**, *9*, 423−340.
(44) Jakubczyk, D.; Derkachov, G.; Do Duc, T.; Kolwas, K.; Kolwas, M. Coefficients of Evaporation and Gas Phase Diffusion of Low-Volatility Organic Solvents in Nitrogen from Interferometric Study of Evaporating Droplets. *J. Phys. Chem. A* **2010**, *114*, 3483−3488.
(45) Jakubczyk, D.; Zientara, M.; Kolwas, K.; Kolwas, M. Temperature dependence of evaporation coefficient for water measured in droplets in nitrogen under atmospheric pressure. *J. Atmos. Sci.* **2007**, *64*, 996−1004.
(46) Jakubczyk, D.; Derkachov, G.; Kolwas, M.; Kolwas, K. Combining weighting and scatterometry: Application to a levitated droplet of suspension. *J. Quant. Spectrosc. Radiat. Transfer* **2013**, *126*, 99−104.
(47) Harvey, A.; Gallagher, J.; Levelt Sengers, J. Revised formulation for the refractive index of water and steam as function of wavelenght, temperature and density. *J. Phys. Chem. Ref. Data* **1998**, *27*, 761−775.
(48) Weber, M., Ed. *Handbook of Optical Materials*; CRC Press: Boca Raton, FL, 2003.
(49) El-Kashef, H. The necessary requirements imposed on polar dielectric laser dye solvents. *Physica B* **2000**, *279*, 295−301.
(50) Eklund, P.; Rao, A.; Wang, Y.; Zhou, P.; Wang, K.; Holden, J.; Dresselhaus, M.; Dresselhaus, G. Optical properties of C_{60}- and C_{70}-based solid films. *Thin Solid Films* **1995**, *257*, 211−232.
(51) Leviton, D.; Frey, B. Temperature-dependent absolute refractive index measurements of synthetic fused silica. *Proc. SPIE* **2006**, *6273*, 62732K.
(52) Steiner, B.; Berge, B.; Gausmann, R.; Rohmann, J.; Rühl, E. Fast *in situ* sizing technique for single levitated liquid aerosols. *Appl. Opt.* **1999**, *38*, 1523−1529.
(53) Berge, B.; Sudholz, B.; Steiner, B.; Rohmann, J.; Rühl, E. *In situ* size determination of single levitated solid aerosols. *Phys. Chem. Chem. Phys.* **1999**, *1*, 5485−5489.
(54) Maeda, M.; Akasaka, Y.; Kawaguchi, T. Improvements of the interferometric technique for simultaneous measurement of droplet size and velocity vector field and its application to a transient spray. *Exp. Fluids* **2002**, *33*, 125−134.
(55) Wilms, J. Evaporation of Multicomponent Droplets. Ph.D. thesis, Universität Stuttgart, 2005.
(56) Jakubczyk, D.; Derkachov, G.; Bazhan, W.; Łusakowska, E.; Kolwas, K.; Kolwas, M. Study of microscopic properties of water fullerene suspensions by means of resonant light scattering analysis. *J. Phys. D* **2004**, *37*, 2918−2924.
(57) Haynes, W. *CRC Handbook of Chemistry and Physics*, 95th ed.; Taylor & Francis: 2014.
(58) Revised Supplemantary Release on Saturation Properties of Ordinary Water Substance; The International Association for the Properties of Water and Steam: St. Petersburg, Russia, 1992.
(59) NIST Chemistry WebBook, Standard Reference Database Number 69; The National Institute of Standards and Technology: Gaithersburg, MD, 2005.
(60) Lugg, G. Diffusion coefficients of some organic and other vapors in air. *Anal. Chem.* **1968**, *40*, 1072−1077.
(61) Air Emissions Models for Waste and Wastewater; U.S. Environmental Protection Agency: 1994.
(62) Diethylene Glycol Product Guide; The MEGlobal Group of Companies: 2005.

(63) Cammenga, H.; Schulze, F.; Theuerl, W. Vapor Pressure and Evaporation Coefficient of Glycerol. *J. Chem. Eng. Data* **1977**, *22*, 131−134.
(64) Davies, J.; Haddrell, A.; Miles, R.; Bull, C.; Reid, J. Bulk, surface, and gas-phase limited water transport in aerosol. *J. Phys. Chem. A* **2012**, *116*, 10987−10998.